Microporous and Mesoporous Materials 378 (2024) 113258

Contents lists available at ScienceDirect

Microporous and Mesoporous Materials

journal homepage: www.elsevier.com/locate/micromeso

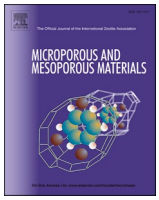

Controlling copper location on exchanged MOR-type aluminosilicate zeolites for methanol carbonylation: *In situ/operando* IR spectroscopic studies

Ligia A. Luque-Álvarez *, Guillermo Torres-Sempere, Francisca Romero-Sarria, Luis F. Bobadilla, Tomás Ramírez-Reina, José A. Odriozola

Departamento de Química Inorgánica e Instituto de Ciencia de Materiales de Sevilla, Centro Mixto CSIC - Universidad de Sevilla, Av. Américo Vespucio 49, 41092, Sevilla, Spain

ARTICLE INFO

Keywords:
Mordenite-zeolites
Cation location
Methanol carbonylation
In situ/operando IR

ABSTRACT

Replacing homogeneous catalytic processes by heterogeneous routes based on the utilization of solid catalysts is of great interest from an environmental point of view. Owing to their genuine pore structure, zeolites such as mordenites (MOR) have emerged as game-changing materials to enable the heterogenization of catalytic processes including methanol carbonylation. Cu-exchange zeolites take the edge over pristine zeolites, leading to enhanced catalytic performance in terms of greater activity, selectivity, and stability. Herein, the overall catalytic activity and stability can be modulated upon controlling the environment and location of copper active sites in zeolites. In this study, Cu-exchanged mordenites were strategically synthesized to investigate the role of Cu location inside of MOR cavities under working conditions by means of *in situ/operando* infrared (IR) spectroscopic studies. The results obtained revealed that a major proportion of Cu in the MR-8 cavities notably enhances the activity and stability of the catalyst. This study provides crucial insights for fine-tuning zeolite catalysts to achieve the heterogenization of homogeneous carbonylation processes.

1. Introduction

The importance of acetic acid as a platform chemical compound within the industrial domain has garnered notable attention. Over recent years, there has been a substantial growth in both the production and commercial distribution of this compound. Currently, approximately 80 % of acetic acid production is accomplished through homogeneous-catalysed carbonylation of methanol, involving the utilization of catalysts based on noble metals alongside halogenated and corrosive promoters. However, transition towards a circular economy to meet the Sustainable Development Goals brings new challenges to chemical processes opening opportunities for the next generation of optimised catalytic process. In particular, new trends in heterogeneously catalysed carbonylation for the sustainable production of acetic acid and derivatives are highly desired and are the subject of inspiring investigations [1]. In this context, catalytic systems such as carbon-based catalysts [2], heteropoly acids [3], oxide-supported transition metals catalysts [4], and immobilized metal complexes catalysts [5] are currently being explored to achieve this objective. Beyond the mentioned materials zeolites, particularly the mordenite (MOR) type are gathering momentum as promising systems for carbonylation processes, due to their enhanced catalytic performance in the reaction [6]. This superior activity is attributed to its intricate porous structure with both size and distribution being suitable for carbonylation goals.

These solids present an orthorhombic structure and a hydrated chemical formula $Na_8Al_8Si_{40}O_{96}\cdot 24H_2O$ with an ideal composition. Thus, they consist of 12-member ring-shaped main cavities along [0 0 1] direction, and 8-membered ring-shaped cavities, commonly referred as side pockets, along the [0 1 0] direction. This system of channels gives rise to specific properties in the different acid sites located in both cavities [7,8]. Various studies have demonstrated that methanol carbonylation selectively takes place within the 8-membered ring (MR-8) cavities of the solid [9], while the 12-membered ring (MR-12) cavities are explicitly designated for facilitating the diffusion of reagents and products [10]. The latter are involved in coke deposition, subsequently leading to the deactivation of the catalyst. Therefore, the active sites for methanol carbonylation are Brønsted sites inside the zeolitic cavity. When placing Cu^+ close to these sites the catalyst activity

* Corresponding author.
E-mail address: llalvarez@us.es (L.A. Luque-Álvarez).

https://doi.org/10.1016/j.micromeso.2024.113258
Received 11 June 2024; Received in revised form 8 July 2024; Accepted 15 July 2024
Available online 16 July 2024

increases and the catalyst is less prone to deactivate [9]. Brønsted sites are located in eight membered rings (MR-8s), connected to 12-membered ring (MR-12s) channels in mordenite. However, methanol carbonylation to acetic acid occurs selectively in the MR-8 pockets while hydrocarbon formation resulting in deactivation is also easier in MR-12 cavities [6,11]. Still, there are evidence of a synergistic effect between copper and zinc in the carbonylation reaction within Cu–Zn-exchanged zeolites. Zn cations are preferentially located in T3 sites of the MR-8 pockets but exchanging H-MOR with Zn and Cu results in the presence of Cu in these sites while Zn^{2+} is now located in the T4 sites of the MR-12 cavities [12].

Furthermore, the zeolite crystallite size, topology and nature affect to the acidity and diffusivity inside the channels, modifying both the activity and the stability of the catalysts [13,14]. Therefore, it may be possible to shift the reaction to the desired products by adjusting the reaction conditions (temperature, pressure, and reactant concentrations) once the catalyst active sites have been carefully designed.

Under these premises and motivated by the need to find new strategies to improve the catalytic performance of exchanged zeolites, the present work evaluates the location of the active sites in the framework of mordenite-type zeolites and its relevance in the catalytic activity. Although some physicochemical properties of catalytic solids can be understood by macroscopic phenomena, a thorough time and space-resolved study is mandatory to shed lights on key structural and dynamic aspects at the molecular level leading to a comprehensive understanding of the role of the active sites [15]. Herein, the application of *in situ/operando* infrared (IR) spectroscopic methods was employed to gain a deeper understanding of individual active sites and the reaction intermediates during methanol carbonylation as central process for acetic acid production via heterogenous catalysis.

2. Materials and methods

2.1. Catalysts synthesis

Commercial ammonium MOR-type (CBV-21A) zeolite with SiO_2/Al_2O_3 ratio of 20, purchased from Zeolyst International and hydrated copper acetate (II) from Panreac were utilized as reagents for the preparation of copper exchanged zeolites.

Two distinct catalysts were obtained from the commercially supplied MOR sample, which initially existed in its ammonic form. In the first synthesis, a calcination process at 600 °C for 3 h with a heating rate of 2 °C min^{-1} was conducted to obtain the protonic form, whereas in the second synthesis, no calcination process was done, and the as-received commercial ammonium sample was directly utilized as parent zeolite. These zeolites were labelled as MOR-600 and MOR-fresh, respectively. After that, a cationic exchange with Cu was conducted using a 0.01 M solution of $Cu(CH_3COO)_2{\cdot}2H_2O$ under stirring during 24 h. Subsequently, the solids were filtered, thoroughly washed, and dried at 100 °C overnight. Finally, the solids were calcined during 3 h at 350 °C using a heating rate of 2 °C min^{-1}. The prepared catalysts were labelled as CuMOR-600 and CuMOR-fresh.

2.2. Characterization techniques

Structural X-ray diffraction (XRD) analysis was performed with a PANalytical X'Pert Pro diffractometer, featuring a Cu Kα anode operating at 40 mA and 45 kV. The diffractograms were acquired within the 2θ range of 10–60°, using a 300 s acquisition time and a 0.05° step width. Structural elucidation was conducted with the PDF2 ICDD2000 database. The Si/Al ratio of zeolites was determined using X-Ray Fluorescence (XRF) on a Zetium Minerals device, while the Cu loading was analysed through Inductively Coupled Plasma-Optical Emission Spectroscopy (ICP-OES) using an iCAP 7200 ICP-OES Duo spectrometer (ThermoFisher Scientific) and digesting the solids in acidic media with a Microwave Digestion System ETHOS EASY (Milestone). The textural properties were evaluated through N_2 physisorption at liquid nitrogen temperature (−196 °C) utilizing a Micromeritics TRIFLEX apparatus specifically tailored for microporous and mesoporous solids. Before adsorption, the samples were degassed for 4 h at 250 °C using a Micromeritics vacuum system. The analysis was conducted via Brunauer–Emmett–Teller (BET) and Barrett–Joyner–Halenda (BJH) methods.

2.3. Catalytic activity tests

A fixed-bed reactor (9 mm i.d.) of Hastelloy stainless steel connected to an automatized microactivity PID Eng&Tech reaction equipment was employed to measure the catalytic activity on the different catalysts. In a typical experiment, ca. 80 mg of solid catalyst with a particle size of 100–200 μm was packed and activated for 1 h at 400 °C passing a flow of 50 mL min^{-1} of 5 vol% O_2/He. Subsequently, the temperature was decreased to 280 °C under He purge, and the pressure was increased to 8 bar. Then, the feed mixture consisting in a CO:methanol mixture with a molar ratio of 5:1 was introduced, and the reaction was performed with a weight space velocity hourly (WHSV) of 11 L g^{-1} h^{-1}. The composition of gas mixture at the inlet and outlet was analysed on-line by gas chromatography using an Agilent 6890 N system equipped with a J&W DB-FATWAX Ultra Inert column. The catalytic activity data was evaluated in terms of methanol conversion and the space–time yield (STY) metric, which is defined as the molar production of methyl acetate/acetic acid per mass of catalyst and per reaction time.

2.4. In situ/operando IR spectroscopic experiments

Three distinct types of IR spectroscopic experiments were performed using a Thermo Nicolet iS50 FTIR spectrometer equipped with a Mercury–Cadmium-Telluride (MCT) detector. Background correction was performed by referencing the ambient conditions in the absence of the sample. All the experiments were carried out in transmission mode using a "sandwich" type reactor cell designed at LCS-Caen (France) [16,17], equipped with a compressed air-cooling system. The cell consists of a stainless-steel cylinder with an annular sample holder in the centre, which holds a self-supporting wafer of 16 mm diameter. The space between each wafer face is filled with KBr windows, and sealing is achieved by using Kalrez O-rings between the windows and the ends of the cell. The IR beam passes perpendicularly through the sample, minimising the dead volume (equal to 0.12 cm^3) and maximising the intensity of the bands due to surface adsorbed species on the catalyst, without superposition of the gas phase. Approximately a wafer of *ca.* 20 mg of catalyst was placed into the cell for each measurement. The spectra were recorded at 128 scans and 4 cm^{-1} of resolution and processed using the OMNIC version 9.0 software. Each experiment can be described as follows: i) In order to establish the temperature at which commercial parent ammonium mordenite is completely transformed into the protonic form, a preliminary *in-situ* IR spectroscopic study of thermal treatment was performed. The commercially as-received ammonia MOR-type zeolite was heated up to 400 °C with a heating rate of 5 °C min^{-1} under Ar flow of 50 mL min^{-1}. During the thermal pretreatment, IR spectra were recorded as a function of temperature. ii) In another study, the location of copper sites was investigated by CO adsorption at 40 °C followed by *in situ* IR spectroscopy. In a typical experiment, the pelletized sample was pretreated through *in-situ* activation at a temperature of 400 °C under an Ar flow of 50 mL min^{-1} to remove impurities and adsorbed water on the solid surface, allowing for a thorough investigation of the hydroxyl region. Subsequently, the temperature was decreased to 40 °C, and 50 mL min^{-1} of 5 vol% CO/Ar flow was passed through the sample for half an hour to observe bands assignable to the interaction of CO with the catalytic surface. iii) Finally, *operando* IR spectroscopic studies were performed to investigate the methanol carbonylation reaction. These experiments were also conducted in transmission mode using the "sandwich-type" cell to analyze

the catalyst surface without gas phase overlapping. Analogously, the pelletized catalyst was pretreated at 400 °C under flow of 50 mL min^{-1} of Ar for 1 h. Then, the catalyst was cooled down to 200 °C and the carbonylation reaction was performed for 1 h at atmospheric pressure by passing through the cell a flow of 30 mL min^{-1} of 17 % v/v of CO in Ar saturated in methanol at 0 °C to achieve a CO:methanol ratio of 3:1. The gas effluents were analysed on-line by mass spectrometry (MS) in a Pfeiffer Vacuum PRISMA PLUS spectrometer, and controlled by QUADERA® software.

3. Results and discussion

3.1. Preliminary in situ IR study: effect of thermal treatment

Fig. 1 displays the evolution of the spectra (a-j) acquired during the thermal treatment of the commercial ammonium MOR-type zeolite. In the initial spectrum recorded at room temperature, two discernible bands are clearly observed: an intense one at 1628 cm^{-1} and another broad band around 3800 - 2500 cm^{-1}. The first band is attributed to physisorbed water interacting with hydroxyl groups in the cavities of the zeolite whereas the latter can be ascribed to both the presence of water and ammonium groups in the zeolitic material. The presence of ammonium groups complicates the IR spectrum as the vibrations of these groups depend on their position in the solid framework, their coordination (multiple H-bonding) with the basic oxygen atoms of the structural network, the Fermi-type resonance interactions in the ν_{NH} region and the combination bands in the bending region [18,19]. In this way, due to the different symmetry, the differentiation of mono- (C_{3v}), bi- (C_{2v}), tri- (C_{3v}/C_s) and tetradentate (C_s) ammonium adsorbed in the Brønsted acid sites is difficult but feasible. With the increasing temperature, the band at 3740 cm^{-1} attributable to the presence of silanols (SiOH) external to the zeolite framework is the first to appear because of ammonium weak interaction with these groups, being desorbed as soon as the thermal treatment initiates. Furthermore, it is also noticed the emergence of a band at 3380 cm^{-1} with the increase of temperature. This feature can be assigned to the stretching vibration of free/-unperturbed N–H groups. In other words, the observation of these bands indicates the presence of tridentate ammonium species. One can see that this band shows a not well-defined shoulder of the band at 3250 cm^{-1}, indicating the prevalence of tetracoordinated species in which all N–H bonds must be engaged in H-bonding interactions, which are not common in zeolitic materials. Their existence and stability require confinement in narrow channels, such as the side pockets of mordenite-type zeolites. Hence, they represent the more stable ammonium species and, consequently, undergo decomposition at higher temperatures. Additionally, two Evans windows can be discerned at 3125 and 2875 cm^{-1}, arising from Fermi-type resonant interactions characteristic of ammonium ions present in the cavities of the solid [18,20,21].

To study the position of ammonium ions within the MOR-type cavities, the difference between the spectra (h-e), corresponding to the

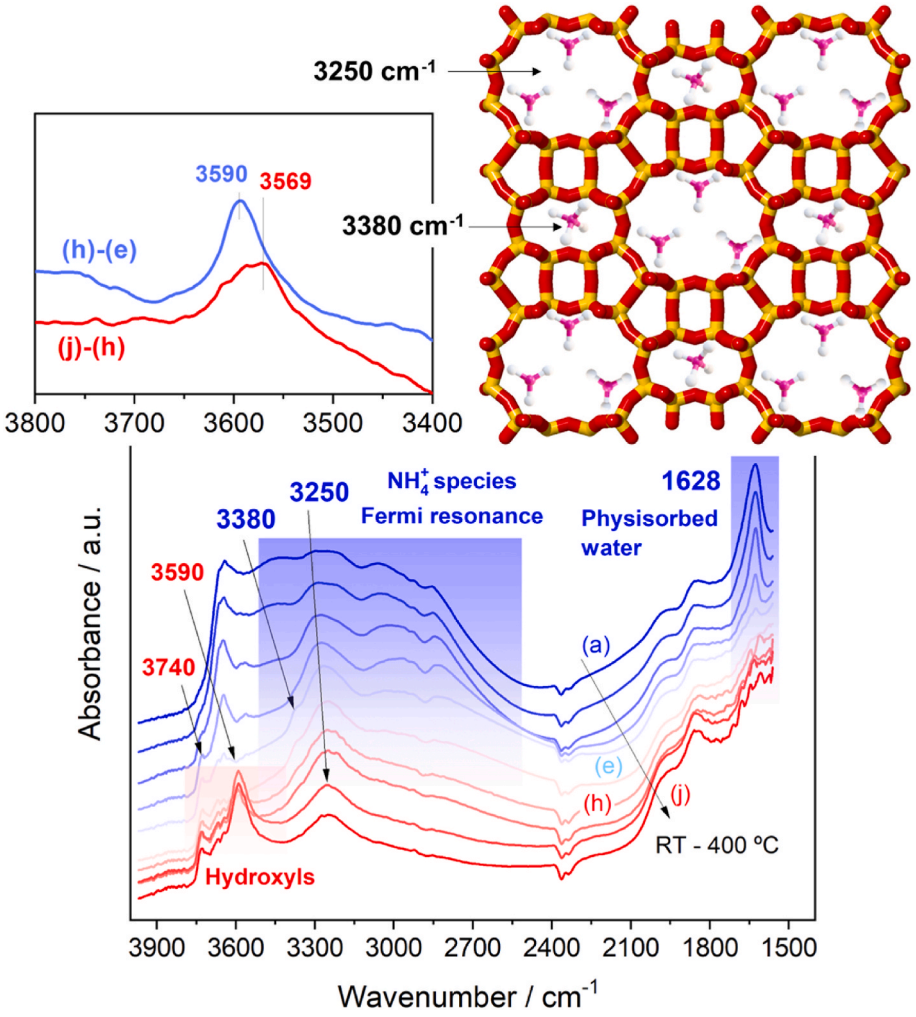

Fig. 1. Evolution of IR spectra with the temperature during thermal treatment of MOR-type fresh zeolite. **Inset:** differences spectra between spectra recorded at 200 °C *(e)*, 300 °C *(h)*, and 400 °C *(j)*. The figure includes a schematic representation of the distribution of ammonium species with different coordination inside of cavities of the zeolite.

disappearance of the band at 3380 cm^{-1}, as well as the difference (j-h), corresponding to the reduction in intensity of the band at 3250 cm^{-1}, were inspected in the hydroxyl region. As shown in Fig. 1 inset, the disappearance of the band at 3380 cm^{-1} (tridentate NH_4^+) is intimately related to the emergence of a band at 3590 cm^{-1}, ascribed to the vibration of hydroxyl groups within the main cavities (MR-12). Concurrently, the diminishing intensity of the band at 3250 cm^{-1} (tetradentate NH_4^+) is intricately tied to the appearance of a band at 3569 cm^{-1}, designated to the vibration of hydroxyl groups within the side pockets (MR-8) of the zeolite [22]. In this way, it can be asserted that tetracoordinated ammonium ions decompose at higher temperatures and are located on the side pockets of mordenite, while tricoordinated ammonium ions are present within the larger cavities. Therefore, it can be concluded that temperatures above 400 °C are required to completely remove the ammonium ions coordinated in both MR-8 and MR-12 cavities to achieve the protonic mordenite. Based on these observations, the commercial ammonium MOR-type (MOR-fresh) was calcined at 600 °C to ensure the complete decomposition of all ammonium species and the production of protonic MOR-type zeolite. Subsequently, copper exchange was performed on both MOR-fresh and MOR-600, and the resulting solids were calcined at 350 °C to decompose the copper precursor salts, resulting in the CuMOR-fresh and CuMOR-600 catalysts.

3.2. Physicochemical properties

Fig. 2a includes the diffraction patterns of both MOR-type of zeolites, while Fig. 2b displays the corresponding diffractograms of both zeolites after cationic-exchange. As intended in the X-Ray patterns, all prepared zeolitic materials showed a mordenite-like crystal structure (JCPDS: 043–0171), being evident the no modification of the crystal structure after thermal treatment. Moreover, there were no diffraction peaks due to metallic copper species nor copper oxides, indicating well-dispersed Cu species. In this way, the procedure for introducing copper into the zeolite pores resulted effective.

Table 1 summarizes the textural properties of all the prepared materials along with the metal loadings and the SiO_2/Al_2O_3 molar ratios determined through ICP-OES and XRF analysis, respectively. Both the total surface area and micropore surface area increase upon copper exchange in all the studied zeolites. This phenomenon may be attributed to the characteristic breathing phenomena exhibited by zeolitic materials when metallic cationic species are introduced inside the cavities of zeolites [23–25]. Additionally, one can notice that the pore volume and pore size are hardly altered with the incorporation of copper and

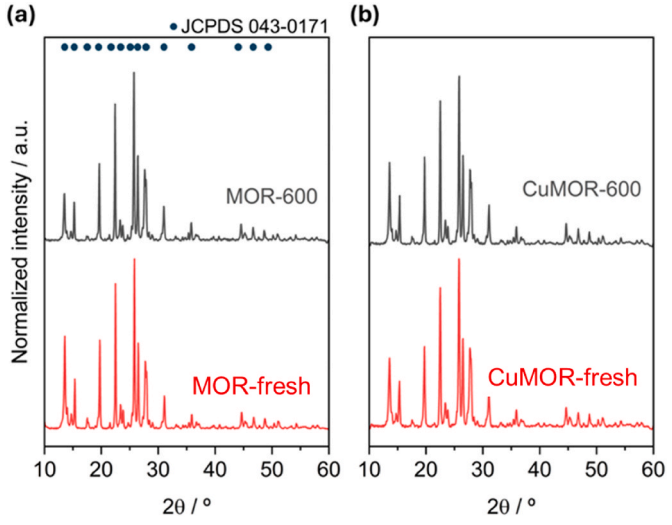

Fig. 2. XRD patterns of the MOR-type zeolites fresh and pretreated at 600 °C before **(a)** and after copper exchanging **(b)**.

preserve the same order of magnitude. Nevertheless, when comparing these catalysts in terms of t-plot micropore surface area is evident from Table 1 that the CuMOR-600 sample has a larger surface area than the other ones. This fact could be related to ammonium ions are more easily exchanged than protons by copper cations in the MR-8 cavities due to confinement factors, in fair agreement with previous reports [26]. Other techniques have confirmed this observation (vide infra). On the other hand, XRF analysis results demonstrate that the SiO_2/Al_2O_3 ratio remains unaltered in comparison with the commercial as-received solid (SiO_2/Al_2O_3 = 20). Likewise, the ICP-OES analysis reveals that the amount of copper exchanged in both protonic form (MOR-600) and ammonic form (MOR-fresh) is closely identical.

3.3. In situ IR dynamic CO adsorption: location of Cu sites

To investigate the location Cu sites in both exchanged CuMOR-600 and CuMOR-fresh catalysts, CO adsorption at 40 °C was performed and followed via *in situ*-IR spectroscopic study. In this way, the catalysts were pretreated at 400 °C for 1 h under Ar flow to remove impurities and water adsorbed in the solid prior to CO adsorption. Fig. 3 shows the IR bands in the 3500–3800 cm^{-1} region ascribed to stretching vibrations of hydroxyl groups in all the samples after thermal treatment. The presence of hydroxyls in the CuMOR-fresh zeolite clearly indicates that ammonium species were decomposed into protons during the thermal treatment. The bands at 3587 and 3607 cm^{-1} are related to the Si(OH)Al bridging Brønsted acid sites inside the side pockets (MR-8) and the main cavities (MR-12), respectively [8], see Fig. 3e. Meanwhile, the band at 3740 cm^{-1} is associated to terminal silanols (SiOH) stretching vibrations, while the bands at 3713 and 3652 cm^{-1} are attributed to defective hydroxyls produced by dealumination of the framework as well as the formation of extraframework Al species during the thermal treatment [27–29]. The fitted Gaussian curves of these bands shown in Fig. 3c and d clearly reveal that the abundance of defective hydroxyl and extraframework Al sites is notably superior in the CuMOR-600 sample. The thermal treatment undertaken at 600 °C in this sample induces the dealumination process in the framework to a greater extent.

Moreover, the relative intensity of the bands at 3607/3587 cm^{-1} shown in Fig. 3b–d provides relevant information on the nature and structural environment of hydroxyl species as well as the location of copper. It is evident that in the CuMOR-600 sample, there is a noticeable decrease in the distribution of hydroxyls in the main cavities (MR-12). This observation suggests that copper was predominantly located in these cavities. Meanwhile, the solid CuMOR-fresh shows a lower concentration of hydroxyls in the side cavities (MR-8), which is associated with a higher concentration of Cu ions in these cavities.

Upon the thermal treatment to achieve a clean surface of the catalysts with exposed hydroxyl groups and Cu sites, the temperature was decreased to 40 °C and a dynamic CO adsorption was performed in both Cu-exchanged solids by passing a flow of 5 % CO/Ar. Fig. 4 shows the evolution of the bands in the CO stretching range in both solids.

As can be noticed, three bands ascribed to copper carbonyl species with distinct coordination geometries are observable. Both bands at 2178 and 2152 cm^{-1} are typical of Cu^+-$(CO)_2$ *gem*-dicarbonyl species while the band at 2156 cm^{-1} is characteristic of Cu^+-CO linear monocarbonyl species [30,31]. To analyze the relative proportion of both types of copper carbonyl species in the two Cu-exchanged mordenites, Fig. 4a–b at the bottom include the deconvoluted spectra recorded after CO saturation at 40 °C. It is clearly evidenced that CuMOR-600 shows a major relative proportion of linear carbonyl species than CuMOR-fresh sample. Previous studies revealed that in MOR-type zeolites, the CO interaction and CO density can be even ten times greater in the MR-8 than in the MR-12 cavities [10], and that Cu^+-NH_4^+ exchange is favoured over Cu^+-H^+ exchange [26]. In agreement, the results discussed above confirm the presence of tetradentate ammonium inside the MR-8 cavities and the existence of more Cu ions in these cavities. In this context, the adsorption of CO suggests that upon introducing CO, more

Table 1
Textural properties of the prepared solids.

Sample	S_{BET} ($m^2\ g^{-1}$)	t-plot micropore surface area ($m^2\ g^{-1}$)	t-plot micropore volume ($cm^3\ g^{-1}$)	Pore size (Å)	Cu loading[a] (wt.%)	SiO_2/Al_2O_3[b]	Cu/Al
MOR-600	429	368	0.19	24	–	23	–
CuMOR-600	478	455	0.19	25	1.7	23	0.1
MOR-fresh	354	311	0.18	25	–	22	–
CuMOR-fresh	423	365	0.19	24	1.6	22	0.1

[a] Determined via ICP-OES analysis and.
[b] Determined via XRF analysis.

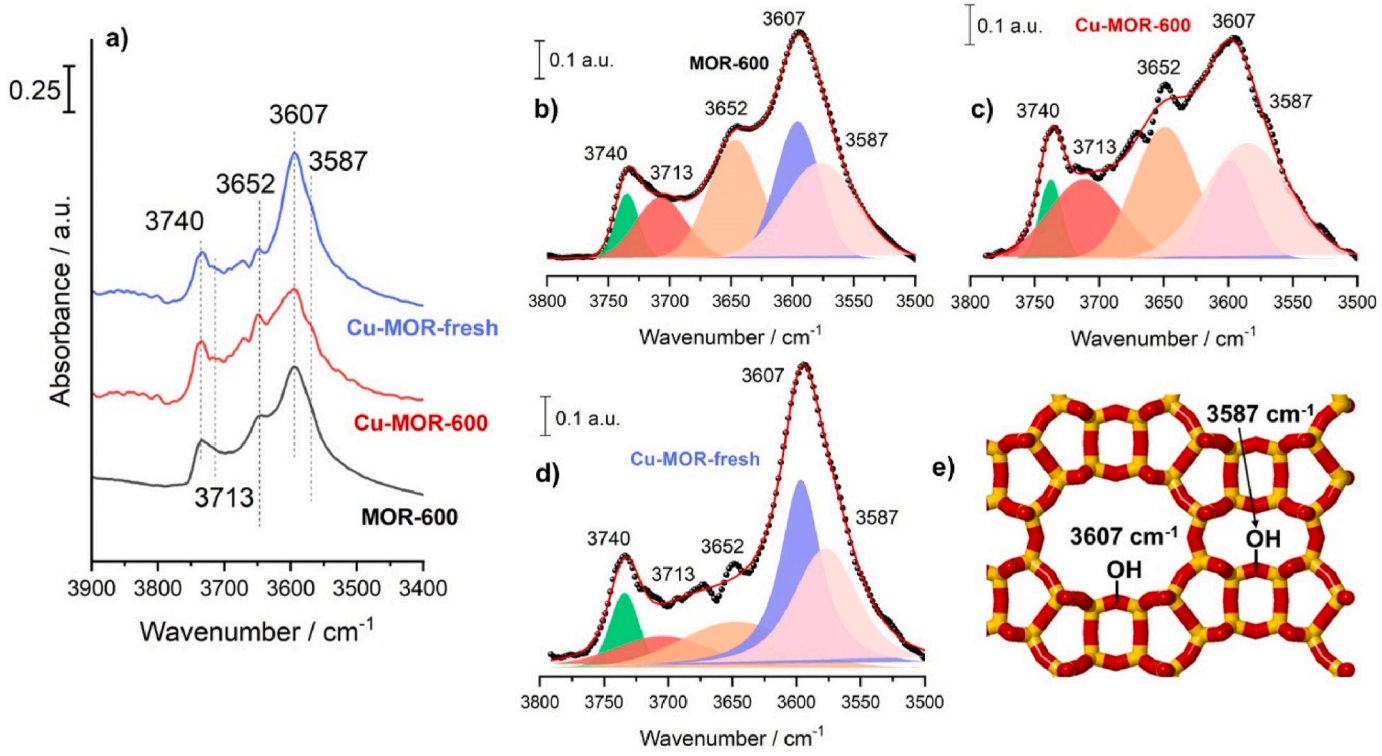

Fig. 3. Stretching vibrations of hydroxyl groups for thermally activated samples **(a),** fitted Gaussian curves for MOR-600 **(b),** CuMOR-600 **(c),** and CuMOR-fresh **(d)** zeolites, and illustration of Si(OH)Al bridging Brønsted acid sites within the side pockets (MR-8) and the main cavities (MR-12) **(e)**.

$Cu^+(CO)_2$ adducts will be formed inside these cavities due to a higher proportion of Cu ions and confinement effects in the side pockets of the CuMOR-fresh zeolite. Finally, it should be mentioned that after CO saturation was feed a purge of Ar at 40 °C and only Cu^+-(CO) species remained on the surface while *gem*-dicarbonyls were rapidly evacuated.

3.4. Catalytic performance in methanol carbonylation

The catalytic activity towards methanol carbonylation reaction of both Cu-exchanged zeolites was evaluated in terms of methanol conversion, and methyl acetate and acetic acid production. As shown in Fig. 5a, the CuMOR-fresh catalyst exhibits stable methanol conversion while CuMOR-600 was drastically deactivated after 5 h of continuous reaction run. It is also evident that CuMOR-fresh presents a higher methanol conversion than CuMOR-600, although this superior conversion is related to a major production of dimethyl ether (Fig. 5a inset) by dehydration of methanol. Analysing the product distribution in Fig. 5b–c, we see that CuMOR-600 shows superior STY of the oxygenated compound of interest, methyl acetate, and acetic acid. However, the production of both valuable chemicals declines sharply after 2 h. By contrast, the CuMOR-fresh catalyst presents lower values of methyl acetate and acetic acid productivity although the production was more stable. It is noteworthy that in both cases methyl acetate was initially produced, and subsequently acetic acid was formed, indicating that the formation of acetic acid results from the hydrolysis of methyl acetate.

Based on these observations, considering that CuMOR-fresh exhibited a higher concentration of Cu ions inside the MR-8 cavities and proved to be the most stable catalyst, it could be inferred that methanol carbonylation to valuable oxygenated compounds predominantly occur in the MR-8 side pockets. Conversely, deactivation appears to be more favoured in CuMOR-600 catalyst, possibly indicating that when the reaction takes place in the MR-12 cavities, hydrocarbon formation and subsequent coke deposition occurs. This finding aligns with previous studies in the field reported elsewhere [6,9,11].

It seems clear that the main challenge with zeolites is their rapid deactivation since they are prone to channels clogging by the formation of coke deposits. Thus, the presence of Cu^+ in close contact to Brønsted sites in confined MR-8 side pockets increases the catalyst activity and makes it less prone to deactivation.

3.5. Operando IR spectroscopic studies: elucidating the reaction mechanism

Operando IR spectroscopy studies were conducted to gain insights into the active sites participating in the methanol carbonylation and the evolution of the intermediates involved in the reaction pathway in the Cu-exchanged zeolites. Fig. 6a–b shows the evolution in time of the IR spectra exhibited by the two Cu-exchanged zeolites during the methanol

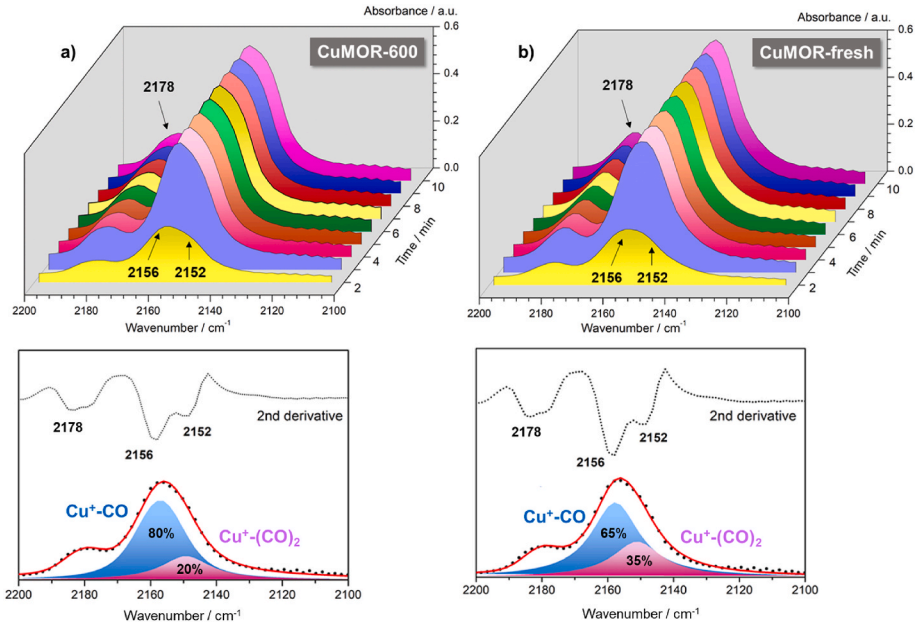

Fig. 4. Evolution of IR spectra in the CO stretching region during the dynamic CO adsorption at 40 °C on thermally activated CuMOR-600 **(a)** and CuMOR-fresh **(b)** zeolites. At the bottom of (a) and (b) are displayed the corresponding deconvoluted spectra recorded after CO saturation for both samples.

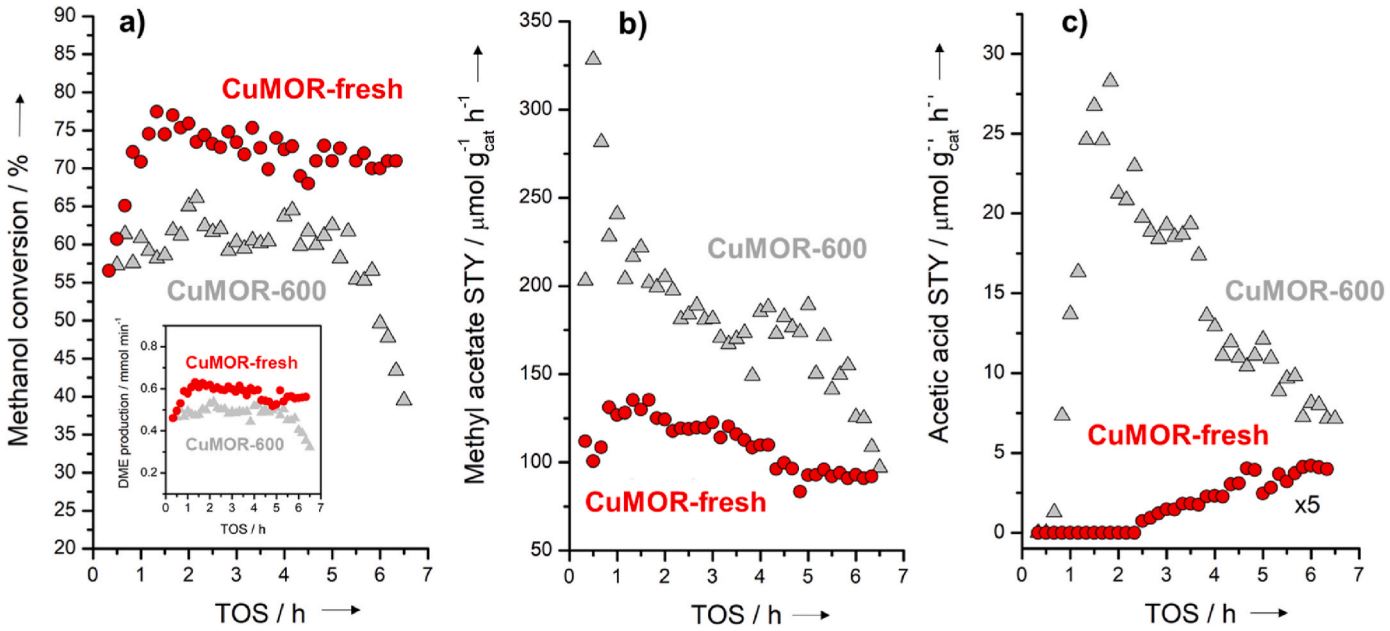

Fig. 5. Evolution of methanol conversion **(a)**, methyl acetate STY **(b)** and acetic acid STY **(c)** as a function of the time-on-stream during methanol carbonylation for both Cu-exchanged zeolites after thermal activation in argon at 400 °C for 1 h. **Inset:** Evolution of DME production. **Reaction conditions:** WHSV = 11 L g^{-1} h^{-1}, T = 280 °C, P = 8 bar and CO/MeOH ratio of 5:1.

carbonylation reaction. An evident disappearance of bands related to hydroxyl groups (3800–3100 cm^{-1}) occurred simultaneously with the emergence of bands in the C–H stretching region (3100–2800 cm^{-1}) in both catalysts. These latter bands are mainly ascribed to ν_{CH} of methoxide species [32] and adsorbed dimethyl ether (DME) produced through methanol dehydration with the acidic hydroxyl groups [33–35], as it is well known that the dehydration of methanol at acid sites is a fundamental step in the reaction. Additionally, several bands in the range 1700–1350 cm^{-1} appeared, characteristic of C═O stretching, C–H bending and C–O stretching vibrations of surface-adsorbed acetyl species [36,37]. The main distinction between both Cu-exchanged zeolites lies in the presence of additional bands at 1610, 1430 and 1375 cm^{-1} with a weak, discernible band at 3230 cm^{-1} in the CuMOR-fresh zeolite. These features are related to acetates and acidic compounds unrevealing the formation of acetic acid [11]. Upon closer inspection of the carbonyl stretching region, Fig. 6a–b inset shows evidence in both cases of the disappearance of features ascribed to copper monocarbonyls species (2156 cm^{-1}) and the evolution of a band at 2133 cm^{-1} which is ascribed to the formation of an acetyl-type copper carbonyl complex [11]. This intermediate is formed by CO insertion into copper adsorbed methoxy groups at low/moderate pressures and may drive the reaction to adsorbed acyl intermediates that further evolve into acetic acid [9]. A similar mechanism has been proposed for the polyoxometalate-based catalysts, in which methoxy groups adsorbed con acid sites react with

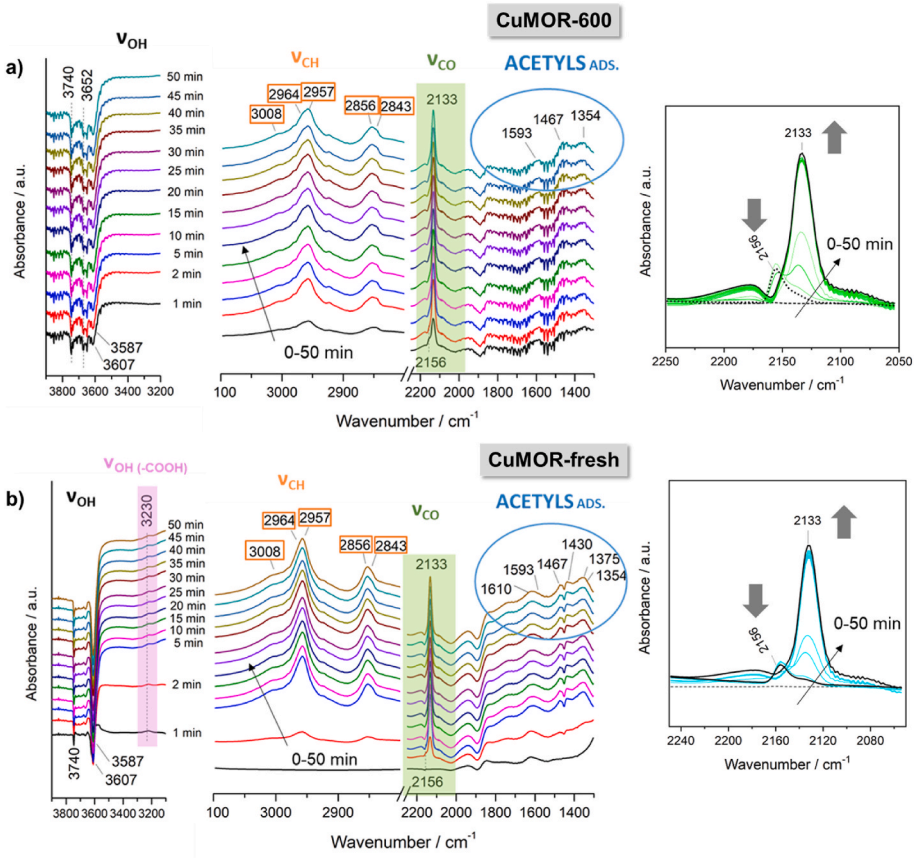

Fig. 6. Time evolution of the IR spectra during the methanol carbonylation reaction at 200 °C and 1 bar on CuMOR-600 **(a)** and CuMOR-fresh **(b)**. **Inset:** Evolution of CO adsorbed species in both Cu-exchanged catalysts.

cationic species that hold CO molecules [38].

Fig. 7 displays the evolution of the gas phase analysed by mass spectrometry during methanol carbonylation and the evolution of the IR bands associated with the most relevant surface species involved in the reaction in both CuMOR-600 (Fig. 7a) and CuMOR-fresh (Fig. 7b).

As can be observed in Fig. 7a, DME production ($m/z = 45$) is accompanied by methanol consumption ($m/z = 31$) and the disappearance of the bands ascribed to the Brønsted acid sites in MR-12 main cavities (3607 cm^{-1}) in the CuMOR-600 sample. This suggests that these hydroxyl groups are actively involved in the methanol dehydration reaction. Another clear correlation evidenced is the disappearance of the band assignable to the external SiOH groups (3740 cm^{-1}) with the appearance of Si–*O*-methyl species (2856 cm^{-1}) [39], which highlights the importance of these groups in the reaction in MOR-type zeolites. These tendencies are also noticeable in the CuMOR-fresh sample (Fig. 7b), although in this case the production of DME is superior. The most noteworthy distinction is related to the presence and evolution of the band at 3230 cm^{-1} attributed to the vibration of OH group in carboxylic acids [40,41], which is only appreciable in the CuMOR-fresh sample. The growth and evolution of this band are evident in Fig. 7b, although the gas phase analysis by MS does not reveal a substantial presence of acetic acid. This observation may be expected due to the

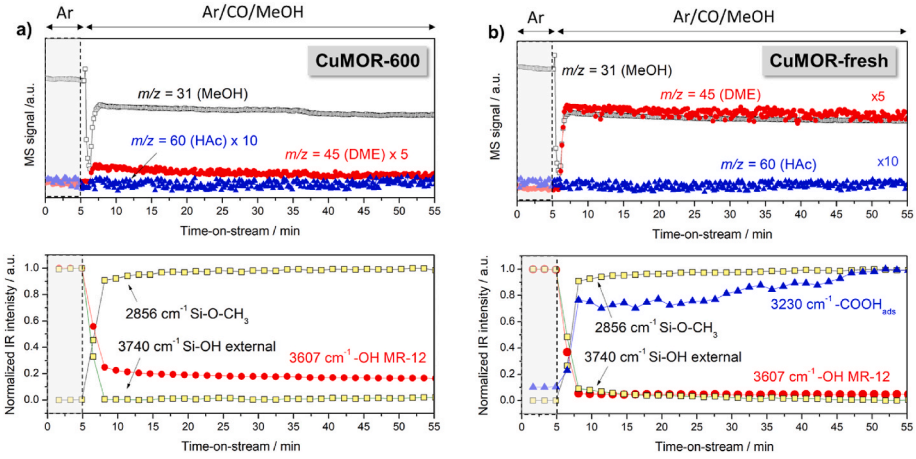

Fig. 7. Evolution of the gas phase followed on-line by MS and evolution of the main bands related to surface species involved in the reaction analysed by *operando* IR spectroscopy in both CuMOR-600 **(a)** and CuMOR-fresh **(b)** catalysts.

very low conversion and potential diffusional limitations in the pellet.

Considering *operando* IR-MS studies and the catalytic performance results, a mechanism for this reaction was proposed, also supported by earlier studies [14,42] and in agreement with reported studies by other authors [11,43]. As illustrated in Fig. 8, methanol dehydration initially occurs at the Brønsted acid centers of both MR-8 and MR-12 cavities, resulting in the formation of dimethyl ether (DME) and methoxides adsorbed on the catalyst surface. Simultaneously, CO activation takes place at the copper redox centers in the MR-8 cavity, leading to the formation of copper monocarbonyls. Subsequently, the methoxide groups are inserted into these carbonyls, generating an acetyl-type intermediate specie. This intermediate reacts with desorbed DME in the gas phase, finally producing methyl acetate. Lastly, the formed methyl acetate undergoes hydrolysis, yielding acetic acid. A schematic mechanism is provided in Fig. 9.

4. Conclusions

Structure-activity correlation is at the heart of catalyst design being a fundamental guiding factor in the pursuit of optimised catalytic materials for multiple applications. In this study, two different copper-exchanged catalysts derived from NH_4-MOR and H-MOR have been prepared and tested with the aim of understanding the location of the active copper sites and subsequently improving the activity and stability of catalysts based on MOR-type zeolites in the methanol carbonylation reaction. With equivalent metal loading for both catalysts, a thermal treatment followed by CO adsorption was employed to assess the distribution of hydroxyls and Cu location, respectively, within the zeolite cavities. This analysis revealed a preference for NH_4↔Cu cation exchange over H↔Cu in the 8-membered ring (MR-8) cavities, which are selectively involved in the targeted reaction. Furthermore, our comprehensive catalytic activity study showcases enhanced activity and stability of the Cu-exchanged catalyst originated from NH_4-MOR in the methanol carbonylation process, leading to the production of acetic acid. *Operando* IR-MS results also provide valuable insights into the bifunctional mechanism followed by these catalysts during the considered reaction. All in all, our work evidences the power of *operando* spectroscopy for heterogenous catalysts design paving the way to exploring promoted mordenites as highly efficient systems for methanol carbonylation and ultimately leading to greener routes for acetic acid production in the context of a circular economy.

CRediT authorship contribution statement

Ligia A. Luque-Álvarez: Writing – original draft, Visualization, Methodology, Investigation, Data curation, Conceptualization. **Guillermo Torres-Sempere:** Visualization, Methodology, Investigation, Conceptualization. **Francisca Romero-Sarria:** Supervision, Methodology, Conceptualization. **Luis F. Bobadilla:** Writing – review & editing, Validation, Supervision, Methodology, Conceptualization. **Tomás Ramírez-Reina:** Writing – review & editing, Funding acquisition. **José A. Odriozola:** Supervision, Funding acquisition.

Declaration of competing interest

The authors declare the following financial interests/personal relationships which may be considered as potential competing interests:

Ligia Amelia Luque Alvarez reports financial support was provided by University of Seville. Jose Antonio Odriozola reports financial support was provided by Spain Ministry of Science and Innovation. If there are other authors, they declare that they have no known competing financial interests or personal relationships that could have appeared to influence the work reported in this paper.

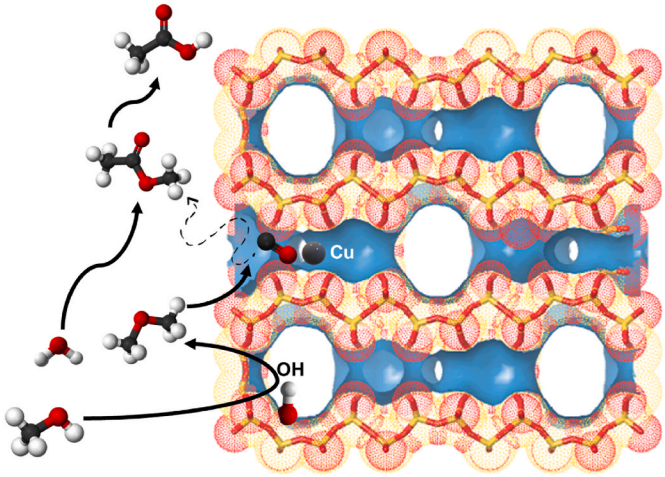

Fig. 8. Proposed reaction mechanism for methanol carbonylation on Cu-exchanged MOR-type zeolite.

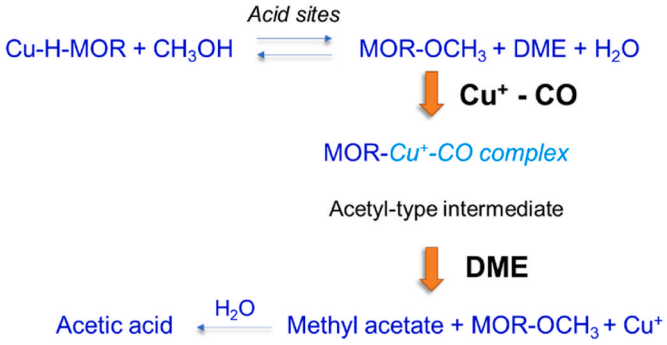

Fig. 9. Schematic methanol carbonylation reaction mechanism on Cu-exchanged MOR zeolites.

Data availability

Data will be made available on request.

Acknowledgments

Financial support for this work has been obtained from the Spanish Ministerio de Ciencia e Innovación through the project SMART-FTS (PID2021-126876OB-I00) sponsored by MCIN/AEI/10.13039/501100011033 and European Union ERDF. Ligia A. Luque Álvarez thanks VI-PPITUS (University of Sevilla) for her current predoctoral contract.

References

[1] L.F. Bobadilla, L. Azancot, L.A. Luque-Álvarez, G. Torres-Sempere, M. González-Castaño, L. Pastor-Pérez, J. Yu, T. Ramírez-Reina, S. Ivanova, M.A. Centeno, J. A. Odriozola, Development of power-to-X catalytic processes for CO_2 valorisation: from the molecular level to the reactor architecture, Chem 4 (2022) 1250–1280, https://doi.org/10.3390/chemistry4040083.

[2] A.Y. Kapran, V.I. Chedryk, L.M. Alekseenko, S.M. Orlyk, Carbonylation of methanol over nickel-copper based supported catalysts, Catal. Lett. 151 (2021) 993–1002, https://doi.org/10.1007/s10562-020-03368-9.

[3] Y. Liu, K. Murata, M. Inaba, Heterogeneous carbonylation of dimethyl ether to methyl acetate over bifunctional catalysts containing Rh and heteropoly acids, React. Kinet. Mech. Catal. 117 (2016) 223–238, https://doi.org/10.1007/s11144-015-0914-4.

[4] J. Qi, J. Finzel, H. Robatjazi, M. Xu, A.S. Hoffman, S.R. Bare, X. Pan, P. Christopher, Selective methanol carbonylation to acetic acid on heterogeneous atomically dispersed ReO_4/SiO_2 catalysts, J. Am. Chem. Soc. 142 (2020) 14178–14189, https://doi.org/10.1021/jacs.0c05026.

[5] K. Park, S. Lim, J.H. Baik, H. Kim, K.D. Jung, S. Yoon, Exceptionally stable Rh-based molecular catalyst heterogenized on a cationically charged covalent triazine framework support for efficient methanol carbonylation, Catal. Sci. Technol. 8 (2018) 2894–2900, https://doi.org/10.1039/c8cy00294k.

[6] M. Boronat, C. Martínez-Sánchez, D. Law, A. Corma, Enzyme-like specificity in zeolites: a unique site position in mordenite for selective carbonylation of methanol and dimethyl ether with CO, J. Am. Chem. Soc. 130 (2008) 16316–16323, https://doi.org/10.1021/ja805607m.

[7] M. Bryan Zambale Gili, M.T. Conato, Synthesis and characterization of mordenite-type zeolites with varying Si/Al ratio, Mater. Res. Express 6 (2018) 015515, https://doi.org/10.1088/2053-1591/aae8db.

[8] O. Marie, P. Massiani, F. Thibault-Starzyk, Infrared evidence of a third brønsted site in mordenites, J. Phys. Chem. B 108 (2004) 5073–5081, https://doi.org/10.1021/jp037915v.

[9] A. Bhan, A.D. Allian, G.J. Sunley, D.J. Law, E. Iglesia, Specificity of sites within eight-membered ring zeolite channels for carbonylation of methyls to acetyls, J. Am. Chem. Soc. 129 (2007) 4919–4924, https://doi.org/10.1021/ja070094d.

[10] Z. Liu, X. Yi, G. Wang, X. Tang, G. Li, L. Huang, A. Zheng, Roles of 8-ring and 12-ring channels in mordenite for carbonylation reaction, From the perspective of molecular adsorption and diffusion 369 (2019) 335–344, https://doi.org/10.1016/j.jcat.2018.11.024.

[11] T. Blasco, M. Boronat, P. Concepción, A. Corma, D. Law, J.A. Vidal-Moya, Carbonylation of methanol on metal–acid zeolites: evidence for a mechanism involving a multisite active center, Angew. Chem. Int. Ed. 46 (2007) 3938–3941, https://doi.org/10.1002/anie.200700029.

[12] A.A.C. Reule, J. Shen, N. Semagina, Copper affects the location of zinc in bimetallic ion-exchanged mordenite, ChemPhysChem 19 (2018) 1500–1506, https://doi.org/10.1002/CPHC.201800021.

[13] G. Bonura, F. Frusteri, C. Cannilla, G. Drago Ferrante, A. Aloise, E. Catizzone, M. Migliori, G. Giordano, Catalytic features of CuZnZr-zeolite hybrid systems for the direct CO_2-to-DME hydrogenation reaction, Catal. Today 277 (2016) 48–54, https://doi.org/10.1016/j.cattod.2016.02.013.

[14] L.A. Luque-Álvarez, M. Serrano-Cruz, M. González-Castaño, L.F. Bobadilla, J. A. Odriozola, Impact of topology framework of microporous solids on methanol carbonylation: an *operando* DRIFTS-MS study, Microporous Mesoporous Mater. 360 (2023) 112725, https://doi.org/10.1016/j.micromeso.2023.112725.

[15] A. Urakawa, Trends and Advances in *Operando* Methodology, 12, 2016, pp. 31–36, https://doi.org/10.1016/j.coche.2016.02.002.

[16] T. Lesage, C. Verrier, P. Bazin, J. Saussey, M. Daturi, Studying the NOx-trap mechanism over a Pt-Rh/Ba/Al_2O_3 catalyst by *operando* FT-IR spectroscopyy, Phys. Chem. Chem. Phys. 5 (2003) 4435–4440, https://doi.org/10.1039/b305874n.

[17] S. Rousseau, O. Marie, P. Bazin, M. Daturi, S. Verdier, V. Harlé, Investigation of methanol oxidation over Au/catalysts using *operando* IR spectroscopy: determination of the active sites, intermediate/spectator species, and reaction mechanism, J. Am. Chem. Soc. 132 (2010) 10832–10841, https://doi.org/10.1021/JA1028809/SUPPL_FILE/JA1028809_SI_001.PDF.

[18] A. Zecchina, L. Marchese, S. Bordiga, C. Pazè, E. Gianotti, Vibrational spectroscopy of NH_4^+ Ions in zeolitic materials: an IR study, J. Phys. Chem. B 101 (1997) 10128–10135, https://doi.org/10.1021/jp9717554.

[19] T. Bučko, J. Hafner, L. Benco, T. Buč Ko, J. Hafner, L. Benco, Adsorption and vibrational spectroscopy of ammonia at mordenite: ab initio study, J. Chem. Phys. 120 (2004) 10263–10277, https://doi.org/10.1063/1.1737302.

[20] D. Perra, N. Drenchev, K. Chakarova, M.G. Cutrufello, K. Hadjiivanov, Remarkable acid strength of ammonium ions in zeolites: FTIR study of low-temperature CO adsorption on NH_4FER, RSC Adv. 4 (2014) 56183–56187, https://doi.org/10.1039/C4RA12504E.

[21] M.F. Claydon, N. Sheppard, The nature of “A,B,C”-type infrared spectra of strongly hydrogen-bonded systems; Pseudo-maxima in vibrational spectra, J. Chem. Soc. D Chem. Commun. (1969) 1431–1433, https://doi.org/10.1039/C29690001431.

[22] S. Bordiga, C. Lamberti, F. Bonino, A. Travert, F. Thibault-Starzyk, Probing zeolites by vibrational spectroscopies, Chem. Soc. Rev. 44 (2015) 7262–7341, https://doi.org/10.1039/c5cs00396b.

[23] M. Alhamami, H. Doan, C.-H. Cheng, A review on breathing behaviors of metal-organic-frameworks (MOFs) for gas adsorption, Materials 7 (2014) 3198–3250, https://doi.org/10.3390/ma7043198.

[24] A.J. Knorpp, A.B. Pinar, M.A. Newton, T. Li, A. Calbry-Muzyka, J.A. Van Bokhoven, Copper-exchanged large-port and small-port mordenite (MOR) for methane-to-methanol conversion, RSC Adv. 11 (2021) 31058–31061, https://doi.org/10.1039/d1ra04643h.

[25] V.M. Georgieva, E.L. Bruce, M.C. Verbraeken, A.R. Scott, W.J. Casteel, S. Brandani, P.A. Wright, Triggered gate opening and breathing effects during selective CO_2 adsorption by merlinoite zeolite, J. Am. Chem. Soc. 141 (2019) 12744–12759, https://doi.org/10.1021/jacs.9b05539.

[26] Y. Wang, H. Zheng, Z. Li, Effect of NH_4^+ exchange on CuY catalyst for oxidative carbonylation of methanol, Cuihua Xuebao/Chinese J. Catal. 37 (2016) 1403–1412, https://doi.org/10.1016/S1872-2067(16)62490-7.

[27] P.A. Jacobs, W.J. Mortier, An attempt to rationalize stretching frequencies of lattice hydroxyl groups in hydrogen-zeolites, Zeolites 2 (1982) 226–230, https://doi.org/10.1016/S0144-2449(82)80056-0.

[28] M. Armandi, B. Bonelli, E. Garrone, M. Ardizzi, F. Cavani, L. Dal Pozzo, L. Maselli, R. Mezzogori, G. Calestani, FT-IR spectroscopic and catalytic study of de-aluminated H-mordenites as environmental friendly catalysts in the hydroxymethylation of 2-methoxyphenol with formaldehyde in aqueous medium, Appl. Catal. B Environ. 70 (2007) 585–596, https://doi.org/10.1016/j.apcatb.2005.12.030.

[29] N.S. Nesterenko, F. Thibault-Starzyk, V. Montouillout, V.V. Yuschenko, C. Fernandez, J.P. Gilson, F. Fajula, I.I. Ivanova, Accessibility of the acid sites in dealuminated small-port mordenites studied by FTIR of co-adsorbed alkylpyridines and CO, Microporous Mesoporous Mater. 71 (2004) 157–166, https://doi.org/10.1016/j.micromeso.2004.03.028.

[30] M.A. Newton, A.J. Knorpp, V.L. Sushkevich, D. Palagin, J.A. Van Bokhoven, Active sites and mechanisms in the direct conversion of methane to methanol using Cu in zeolitic hosts: a critical examination, Chem. Soc. Rev. 49 (2020) 1449–1486, https://doi.org/10.1039/C7CS00709D.

[31] C. Lamberti, S. Bordiga, A. Zecchina, M. Salvalaggio, F. Geobaldoc, C. Otero, A. Nd, XANES, EXAFS and FTIR characterization of copper-exchanged mordenite, J. Chem. Soc., Faraday Trans. 94 (1998) 1519–1525.

[32] T. He, X. Liu, S. Xu, X. Han, X. Pan, G. Hou, X. Bao, Role of 12-ring channels of mordenite in DME carbonylation investigated by solid-state NMR, J. Phys. Chem. C 120 (2016) 22526–22531, https://doi.org/10.1021/acs.jpcc.6b07958.

[33] Z. Azizi, M. Rezaeimanesh, T. Tohidian, M.R. Rahimpour, Dimethyl ether: a review of technologies and production challenges, Chem. Eng. Process. Process Intensif. 82 (2014) 150–172, https://doi.org/10.1016/j.cep.2014.06.007.

[34] A. Brunetti, M. Migliori, D. Cozza, E. Catizzone, G. Giordano, G. Barbieri, Methanol conversion to dimethyl ether in catalytic zeolite membrane reactors, ACS Sustain. Chem. Eng. 8 (2020) 10471–10479, https://doi.org/10.1021/acssuschemeng.0c02557.

[35] F.E. Celik, T. Kim, A.N. Mlinar, A.T. Bell, An investigation into the mechanism and kinetics of dimethoxymethane carbonylation over FAU and MFI zeolites, J. Catal. 274 (2010) 150–162, https://doi.org/10.1016/j.jcat.2010.06.015.

[36] R.P. Young', Infrared spectroscopic studies of adsorption and catalysis. Part 3. Carboxyllic acids and their derivatives adsorbed on silica, Can. J. Chem. 47 (1969) 2237.

[37] A.N. Siyal, S.Q. Memon, M.Y. Khuhawar, Recycling of styrofoam waste: synthesis, characterization and application of novel phenyl thiosemicarbazone surface, Pol. J. Chem. Technol. 14 (2012) 11–18, https://doi.org/10.2478/V10026-012-0095-0.

[38] A. Kumar, S. Mazumder, Toward simulation of full-scale monolithic catalytic converters with complex heterogeneous chemistry, Comput. Chem. Eng. 34 (2010) 135–145, https://doi.org/10.1016/J.COMPCHEMENG.2009.05.018.

[39] I.E. Wachs, Number of surface sites and turnover frequencies for oxide catalysts, J. Catal. 405 (2022) 462–472, https://doi.org/10.1016/J.JCAT.2021.12.032.

[40] H. Yao, Q. Dai, Z. You, Fourier Transform Infrared Spectroscopy characterization of aging-related properties of original and nano-modified asphalt binders, Construct. Build. Mater. 101 (2015) 1078–1087, https://doi.org/10.1016/J.CONBUILDMAT.2015.10.085.

[41] İ.M. Hasdemir, E. Yılmazoğlu, S. Güngör, B. Hasdemir, Adsorption of acetic acid onto activated carbons produced from hazelnut shell, orange peel, and melon seeds, Appl. Water Sci. 12 (2022) 1–13, https://doi.org/10.1007/S13201-022-01797-Y/FIGURES/9.

[42] L.A. Luque-Álvarez, J. González-Arias, F. Romero-Sarria, T.R. Reina, L.F. Bobadilla, J.A. Odriozola, Mechanistic insights into methanol carbonylation to methyl acetate over an efficient organic template-free Cu-exchanged mordenite, Catal. Sci. Technol. 14 (2024) 128–136, https://doi.org/10.1039/d3cy01271a.

[43] M. Boronat, C. Martínez, A. Corma, Mechanistic differences between methanol and dimethyl ether carbonylation in side pockets and large channels of mordenite, Phys. Chem. Chem. Phys. 13 (2011) 2603, https://doi.org/10.1039/c0cp01996h.